Chapter

Four-Dimensional Flow Magnetic Resonance Imaging and Applications in Cardiology

Patrick Geeraert, Hansuk Kim, Safia Ihsan Ali, Ashifa Hudani, Shirin Aliabadi, Monisha Ghosh Srabanti, Hourieh Jamalidinan and Julio Garcia

Abstract

Blood flow through the heart and great vessels moves in three dimensions (3D) throughout time. However, the assessment of its 3D nature has been limited in the human body. Recent advances in magnetic resonance imaging (MRI) allow for the comprehensive visualization and quantification of in-vivo flow dynamics using four-dimensional (4D) flow MRI. In addition, this technique provides the opportunity to obtain advanced hemodynamic biomarkers such as vorticity, helicity, wall shear stress (WSS), pressure gradients, viscous energy loss (EL), and turbulent kinetic energy (TKE). This chapter will introduce 4D flow MRI which is currently used for blood flow visualization and advanced quantification of cardiac hemodynamic biomarkers. We will discuss its advantages relative to other in-vivo flow imaging techniques and describe its potential clinical applications in cardiology.

Keywords: Cardiac flow, 4D flow MRI, hemodynamic biomarkers, and flow quantification

1. Introduction

Imaging and quantifying various characteristics of blood flow throughout the heart is essential in modern-day cardiology. Measuring blood velocities, pressure gradients, regurgitation, stasis (and much more) is one of the most important tools physicians have for diagnosing cardiovascular pathology, stratifying severity, evaluating disease progression, and determining the most effective treatment strategies. Improving the accuracy and depth of such hemodynamic measurements is an ongoing process that continues to enhance clinical success. Two-dimensional phase-contrast magnetic resonance imaging (2D PC-MRI) and Doppler echocardiography are currently the most widely used techniques for measuring cardiovascular blood flow in-vivo [1]. However, while these modalities provide immense value in clinical practice, they have their limitations. Velocity can only be measured in one direction; in Doppler echocardiography following the direction of the ultrasound beam and in 2D PC-MRI following the encoding direction assigned by the user. This can cause errors in flow measurements, depending on whether the beam/plane is placed at the exact location of interest and/or orthogonal to the direction of flow [2, 3].

These 2D measurements often rely heavily on mathematical assumptions that are not always valid [2]. For example, 2D calculations of pressure gradients are known to underestimate pressure recovery downstream of stenosis [4]. In addition, some techniques provide limited viewpoints of the thoracic cavity, such as trans-thoracic echocardiography and trans-esophageal echocardiography [1, 5]. It is also possible to acquire the in-plane velocities (X and Y directions) over time (two velocities + time) or the three plane velocities (X, Y, and Z directions) over time (three velocities + time).

Time-resolved three-dimensional (3D) phase-contrast magnetic resonance imaging (i.e. 4D flow MRI) is a novel non-invasive, non-ionizing imaging technique that provides accurate qualitative and quantitative assessment of blood velocity in all three principle directions [6, 7]. This allows for enhanced accuracy of previously measurable parameters obtained routinely by Doppler echocardiography, such as velocity and reverse flow, as well as the calculation of new parameters, such as wall shear stress (WSS), 3D pressure gradients, and turbulent kinetic energy (TKE). These parameters can be retrospectively visualized and quantified in volumes (rather than cross sections), over the course of a cardiac cycle, and in unlimited viewpoints. Authors can refer to 2D, 3D, 4D, 5D or 7D flow depending on the acquisition scheme used to encode the velocity directions over time. Thus, it is important to understand how the velocity acquisition is defined. In this chapter, 4D flow MRI measures 3 velocity encoded directions in a stack of planes along the cardiac cycle. As such, the ongoing development of 4D flow MRI provides great promise in improving the clinical management of cardiovascular disease.

2. Data acquisition and pre-processing

2.1 Safety and preparation

There are safety measures and recommendations that should be considered for subjects undergoing 4D flow MRI [6, 8]. Patients can fill out pre-imaging safety questionnaires that consider items that can cause a hazard or interfere with the MRI examination. The safety information may become frequently updated because of continuous and rapid changes in the MRI technology. Before starting any cardiac MRI study, compatible electrocardiogram (ECG) leads should be placed on the subject's chest properly. The accurate synchronization of data acquisition with phases of the cardiac cycle, including different stages of contraction and relaxation, is one of the essential requirements for efficacious cardiac MRI exam. This technique is called ECG-gating. A phased-array receiver coil is required to capture the electromagnetic signals needed to create an image. Thus, it is important that receiver coils are positioned appropriately to cover the regions of interest. The use of contrast agents is optional in 4D flow MRI, but they can help increase the signal-to-noise ratio, and therefore improve the image quality.

2.2 Data acquisition

In 4D flow MRI, acquisition parameters (ex: spatial resolution, temporal resolution, field of view, etc.) are optimized and programmed into the scan protocol to provide the best possible imaging accuracy. Setting major scan parameters is primarily a fine balance between adequate temporal/spatial resolution and minimized scan time. Imaging accuracy can also be affected by artifacts (i.e., distortions in the image that are not present in reality), of which velocity encoding (Venc) is an important contributor. Velocity encoding is a user-defined parameter that sets

the upper and lower limits of blood velocity which can be appropriately imaged for within the scan protocol. If the patient's blood velocities fall above the Venc limit, aliasing will corrupt the image with artifacts in those locations. However, if the Venc range is set too high, the image can be populated with noise [9]. Furthermore, artifacts can arise from movement due to cardiac motion and breathing. As shown in **Figure 1**, ECG-gating compensates for cardiac motion to determine when the heart is most still, at which point images are acquired [10]. Simultaneously, diaphragmatic navigator gating compensates for breathing artifacts by similarly tracking movement of the patient's diaphragm and acquiring images at the point of least movement [11]. This allows the patient to breath freely during the scan without creating breathing-related artifacts. These approaches are applied to provide the clearest possible images of 3D global and local blood flow characteristics. Four types of images are produced after acquisition: one magnitude image (shows anatomical structures) and three phase images (shows blood velocity along the Venc directions, often x, y, and z axes).

The most important limiting factor for adding 4D flow to a routine clinical cardiac MRI exam is long scan times associated with multidimensional imaging over the entire cardiac cycle. In 1990s, the total scan time was roughly 40–80 minutes which made difficult its routine application in clinical settings. In recent years, scan times have been further reduced due to ongoing progress in advanced imaging techniques. Nowadays, different reconstruction techniques (parallel imaging, radial and Cartesian sampling, compressed sensing, etc.), in addition to enhanced computing power, have reduced the scan time to 3–10 minutes [12–14]. The latter is facilitating is penetration as a diagnostic tool. Finally, all acquired data are saved in the Digital Imaging and Communications in Medicine standard format in the MRI system database.

2.3 Pre-processing and correction

Due to a range of errors, image quality can be damaged by various factors including noise, eddy current effects, concomitant gradient field effects (Maxell terms), velocity aliasing, and gradient field nonlinearity. Data pre-processing is applied to rectify these potential errors using several correction strategies to make 4D flow MRI a reliable source of 3D flow visualization and quantification, as illustrated in

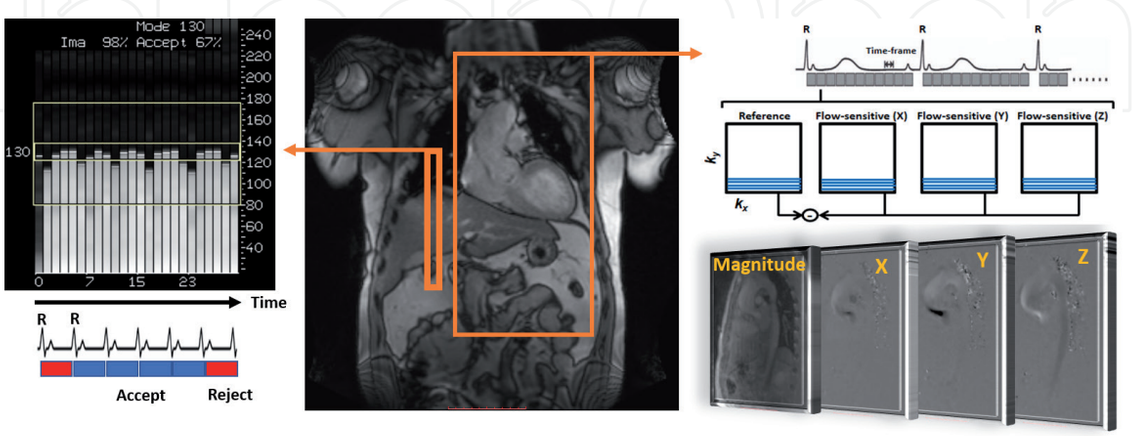

Figure 1.
Data acquisition for 4D flow MRI. *Data acquisition covering the whole heart (large orange rectangle) is acquired using electrocardiogram-gating and respiratory control (small orange rectangle). Three-dimensional velocity-encoding (right side) is used to obtain velocity-sensitive phase images which are subtracted from reference images to calculate blood flow velocities along all three spatial dimensions (X, Y, Z) and averaged magnitude visualizing anatomy over the cardiac cycle.*

Figure 2 [15]. Three-dimensional phase-contrast magnetic resonance angiography (3D PC-MRA) can be obtained at this stage based on acquired data from 4D flow MRI by several presented strategies without the need for further MRI acquisition. A 3D PC-MRA can display complex vascular structures and geometries of interest without requiring a contrast agent. It is vastly helpful in some situations, such as patients with contrast agent contraindication. In addition, 3D PC-MRA allows the user to retrospectively isolate specific volumes of interest for analysis.

However, 4D flow MRI images present difficulties for segmentation algorithms due to extensive variability in cardiovascular structure, geometric intricacy, low resolution, high background noise and motion artifacts. For that reason, manual segmentation remains a widely used method, but manual segmentation takes a long time to perform and is prone to observer variability [16]. There are some established semi-automatic segmentation methods [17–19] which are faster than manual segmentation, nevertheless they are still operator dependent. Recent machine learning and artificial intelligence strategies have shown great ability to solve 4D flow MRI segmentation problems [20]. Machine learning algorithms are powerful techniques that train a machine (i.e. computer) to perform a specific task. Convolutional neural networks (CNNs), which is one of the deep learning techniques, forms the foundation of image segmentation. U-Net is a CNN that was developed specifically for medical image segmentation [21]. Several recent studies that focused on advancing imaging segmentation techniques. Berhane et al. developed a CNN model to segment the aorta from 4D flow MRI images [22]. The performance in this study was compared with manual segmentations, and they reported good agreement across flow and diameter along the aorta. Segmentation speed was <1 second per case, while manual segmentation required at least 360 seconds. Bratt et al. suggested a network based on the U-net and residual modules [23]. They reported similar segmentation performance, < 0.6 seconds per case, however the manual segmentation required 238 seconds per case. Wu et al. developed a combinatorial network for segmenting the left ventricle (LV) [24]. They claimed that combining networks can increase the accuracy of the segmentation.

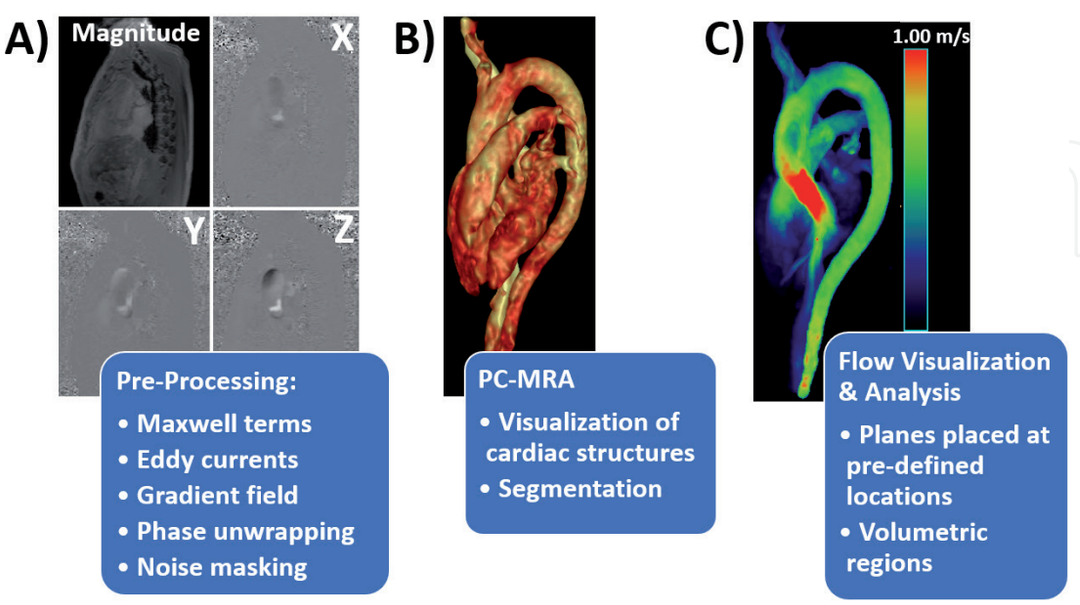

Figure 2.
Data pre-processing. *Acquired 4D flow images are pre-processed applying multiple corrections (panel A). A phase-contrast angiogram (PC-MRA) is calculated to visualize the cardiac structures and can be used for individual segmentation of vessels, panel B. the generated PC-MRA and/or segmentation can be used to mask the velocity field for appropriate visualization and analysis using planes or volumetric regions of interest, panel C. In this example a 58-year-old control volunteer is presented.*

2.4 Flow visualization and quantification

Before flow visualization and quantification, general data quality control, including visual inspection and quantitative quality control, is recommended to ensure internal data is consistent and accurate. Dedicated visualization and quantification software can be used for obtaining streamlines, pathlines, volume rendering, and/or maximum intensity projection (MIP). Streamlines represent a blood particle's instantaneous path tangential to the velocity vector at a particular point of time, such as at peak systole. Pathlines represent a blood particle's path over time (i.e. trajectory). Volume rendering allows us to represent voxel-by-voxel values in a dynamic spatial manner, given access to the entire field of view. A MIP is a single-plane image representing the maximum values through a given direction of the volume, similar to an X-ray image. Taken together, these flow visualization techniques reveal a wealth of information about blood flow abnormalities and cardiovascular disease progression. One of the most significant advantages 4D flow MRI is the ability to retrospectively quantify cardiac flow parameters within specified regions of interest. Flow can be analyzed within a specific volume that has been isolated via segmentation, or via a 2D cross-sectional analysis plane placed within a volume of interest. These analysis planes can be flexibly placed at any anatomical location to quantify general and advanced blood flow parameters. Some of these visualization and quantification methods will be illustrated in the following section.

3. Applications in cardiology

3.1 Congenital heart disease

Eight out of every 1000 infants are born with congenital heart disease (CHD), which encompasses all structural heart defects present at birth, including the great vessels and cardiac valves [25]. Individuals with CHD may develop many cardiac complications, even after surgical correction of the abnormality, including valve insufficiency, arrhythmias, and heart failure [25]. Tetralogy of Fallot is one of the most common forms of cyanotic ("blue baby") CHD, accounting for about 10% of all CHD [26]. Tetralogy of Fallot involves a combination of four defects including right ventricular hypertrophy, aortic override, pulmonary stenosis, and a ventricular septal defect. These patients undergo multiple repeat surgeries and procedures over their lifetime but the hemodynamic factors contributing to the optimal quality of life and outcomes are understudied and poorly understood. Congenital heart disease can benefit from 4D flow MRI via the calculation of advanced hemodynamic parameters, such as WSS, TKE, 3D pressure mapping, and energy loss [5]. For demonstration, we primarily focus on pressure mapping, but **Table 1** provides an overview of 4D flow MRI hemodynamics in CHD.

Fluid pressure measured within the cardiovascular system is widely used in CHD diagnosis, such as coarctation of the aorta, pulmonary hypertension, or atrio-ventricular septal defects. The pressure difference across structural abnormalities (ex: stenosis or ventricular septal defect) or within the LV can reveal much about the severity of the disease. Pressure mapping, based on the measured 3D blood flow velocity field, can be calculated by solving the Navier–Stokes equation, which describes the time-varying flow of a viscous, incompressible Newtonian fluid [33, 34]. This method allows for the estimation of temporally and spatially distributed pressure gradients and across a large vessel segment or cardiac chamber, **Figure 3**. Overall, 3D pressure mapping allows us to gain a better understanding of

Region	CHD type	Conventional flow parameters	Advanced flow parameters	References
Venous return	Fontan/single Ventricle	Collateral flow volume, peak velocity, valvular flow volume	KE, EL, flow connectivity distribution	[5, 8, 27, 28]
	Tetralogy of Fallot	Right heart (RA, RV, PA) systolic peak velocity, net flow, retrograde flow	WSS, vorticity, KE, EL, TKE, pressure drop	[5, 7, 8, 27–29]
Heart wall	Atrial Ventricular Septal Defects	Flow volume, shunt flow volume, shunt ratio	Vorticity, KE, EL, WSS	[5, 8]
Aortic valve	Bicuspid Aortic Valve	Net flow, regurgitation volume, peak velocity	WSS, turbulence, EL, pressure mapping, helicity, flow eccentricity, PWV	[5, 7, 8, 27, 28, 30]
	Marfan Syndrome	AV Peak flow, AV flow volumes	WSS, helical flow, PWV, pressure mapping	[8, 30, 31]
Outflow tracts	Dextro Transposition of the Great Arteries	Net flow volumes, flow ratio, peak velocity	WSS, helical flow	[5, 8]
	Aortic Coarctation	Collateral flow volume, peak velocity across stenosis	Pressure mapping, EL, WSS, helical flow	[5, 8, 27, 30, 32]

CHD: congenital heart disease; AV: aortic valve; RA: right atrium; RV: right ventricle; PA: pulmonary artery; EL: viscous energy loss; KE: kinetic energy; PWV: pulse wave velocity; TKE: turbulent kinetic energy; WSS: wall shear stress.

Table 1.
Overview of research on conventional and advanced 4D flow–derived hemodynamic parameters in CHD.

the basic determinants of time-varying flow in healthy and diseased hearts, which has the potential to improve our methods for diagnosing, treating, and surgically correcting CHD [35, 36].

3.2 Mitral regurgitation

Approximately 10% of the general population will develop mitral regurgitation (MR) throughout their lifetime [37]. Mitral regurgitation is defined as systolic retrograde flow from the LV into the left atrium (LA). The main causes are classified as primary (structural or degenerative abnormality of mitral valve apparatus) or secondary (a disease of the LV interferes with function and integrity of mitral valve apparatus) [38]. This disorder generally progresses insidiously, as the heart compensates for increasing regurgitant volume via LA enlargement that partially relieves LV overload. Long-standing regurgitation yields poor outcomes as it may lead to progressively more severe regurgitation, LV failure, pulmonary hypertension, atrial fibrillation (AF), stroke, and death [39]. If MR is severe, surgery is the recommended treatment to prevent heart failure [1]. Thus, early detection and assessment is crucial, especially in elderly patients who are often ineligible for surgical intervention.

Doppler echocardiography is the most widely used tool for the assessment of MR. The commonly considered parameters when classifying MR severity are jet area, width of vena contracta, effective regurgitant orifice area, regurgitant volume,

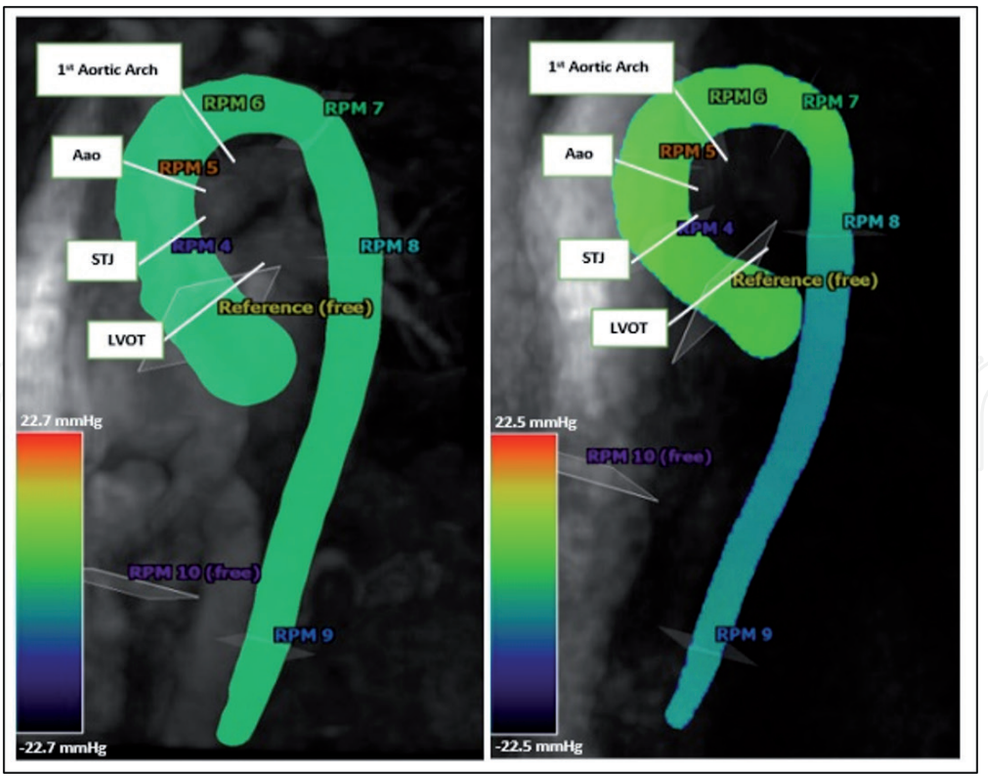

Figure 3.
Pressure mapping. *Volume rendering maps of a control (left) and a patient with repaired tetralogy of Fallot (right). Several analysis planes, including location reference. Reference plane for pressure is in yellow. RPM indicates analysis plane. LVOT: Left ventricular outflow tract; STJ: Sinotubular junction; AAo: Ascending aorta.*

and regurgitant fraction. However, the accuracy of standard approaches used to quantify these parameters can be influenced by the mechanism of regurgitation, direction of the jet, jet momentum, LV loading condition, LA size, and the patient's blood pressure [40, 41]. It is also important to keep in mind that these standard-of-care diagnostic tools do not permit a comprehensive in-vivo assessment of 3D blood flow which is critical to the study of complex 3D hemodynamics surrounding MR. Cardiac MRI has recently been reported as a more accurate tool for quantification of MR flow characteristics and severity grading [42, 43]. Advanced measures of vortex formation, helical flow patterns, EL, pressure mapping, and WSS have shown usefulness for assessment of valve-related disease using 4D flow MRI [44]. The shape of vortex cores have been shown to closely resemble the valve shape, while the vortex's orientation is related to the LV inflow direction [45]. In demonstrating how to extract vortex information from 4D flow MRI, Krauter et al. showed that vortex shape, vorticity and kinetic energy (KE) strongly correlate with transmitral peak velocities [46]. Helical grade was also associated with systolic anterior motion of the mitral valve. Lastly, as shown in **Figure 4**, MR disturbs organized flow, resulting in a reduced contribution of left pulmonary veins to the vortical flow, potentially leading to less efficient ventricular filling and stasis [47].

It is important to note, however, that flow-based biomarkers still require further exploration before they can be reliably applied to daily clinical practice. The construction of 'atlases' that depict physiologically normal blood flow patterns through the LA shows great promise in helping identify the clinical utility of certain hemodynamic parameters and personalizing diagnoses. Normally, MR treatment is primarily based on chamber dimensions and qualitative regurgitation severity grading [48], but it is well recognized that these measures may be insufficient to guide treatment strategies and require multi-modality integration. Four-dimensional flow

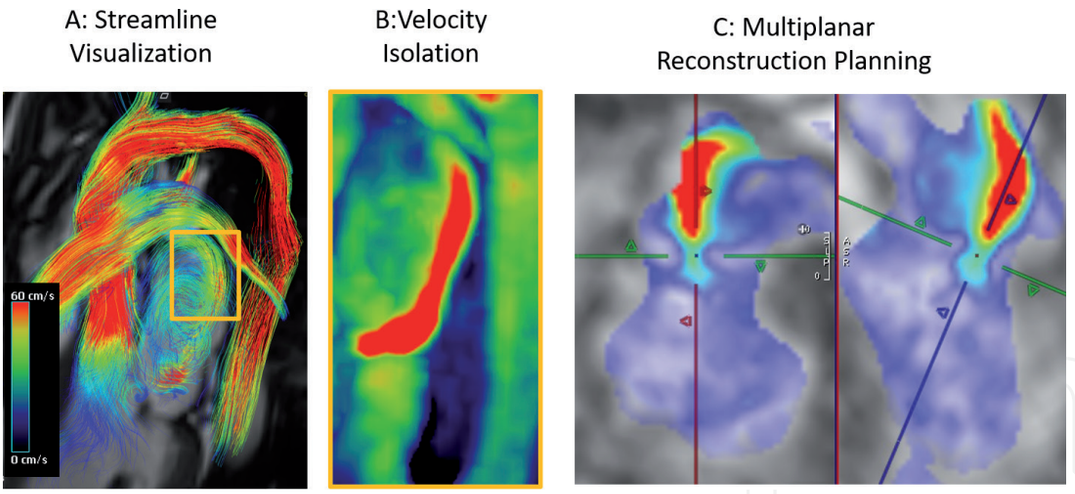

Figure 4.
Mitral regurgitation. *The presented case has mitral thickening with evidence of cleft in the anterior mitral leaflet. Panel A shows a whole heart streamline visualization used to locate mitral regurgitation (orange box). Panel B shows the velocity volume rendering of the velocity field. The mitral regurgitant jet was highly eccentric into the atrial wall. Panel C illustrates the multiplanar reconstruction of the velocity field which allows multiple views of the regurgitant jet. Evaluation led to a mild regurgitation grading with a regurgitant fraction of 15%.*

MRI has provided the ability to construct time-averaged 3D hemodynamic maps (i.e. atlases) from healthy subjects, which can then be used as a reference when evaluating a patient's MR severity. For example, Goffic et al. recently developed strategies for the generation of KE and helicity atlases [49]. Their preliminary data suggest that these atlases may provide insight into hemodynamic influence on LV dysfunction progression and, thus, could have implications on personalized assessment of MR. Such atlases can be created for any hemodynamic parameter of interest and will be further elaborated on in the aortic diseases section of this chapter.

3.3 Atrial fibrillation

Atrial fibrillation is an abnormally fast heart rhythm with uncoordinated atrial activation and ineffective atrial contraction [50, 51]. Multiple simultaneous electrical signals firing within the atria lead to irregular ECG patterns and atrial activity, loss of coordinated atrial contractions, and inadequate ventricular filling. It is classified according to the duration of episodes. At an early stage, an episode of AF terminates within 7 days of onset and sinus rhythm is restored (paroxysmal AF). However, as severity progresses, the AF episode may last beyond one week (persistent AF) or does not terminate (permanent AF). The most common complication of AF is thromboembolic events such as stroke [50, 51]. Reduced LA function increases the risk of blood stasis and clot formation in the LA, especially the left atrial appendage (LAA) which is a small extension of the LA. The CHA_2DS_2-VASc score (accounts for patient history of: Congestive heart failure, Hypertension, Age > 75 years, Diabetes mellitus, Stroke, Vascular disease, Age between 65 and 74 years, and Sex) is currently recommended for stroke risk stratification for AF patients, based on clinical factors such as age, gender, and disease history [50–52]. This risk score is used to recommend the use of anticoagulants and further therapy. However, the score does not contain other individual physiologic factors, so prediction power is limited.

There have been efforts to improve diagnosis and evaluation of disease and risk-assessment of AF through analysis based on 4D flow measurements (**Table 2**). Although some contradictory reports exist, most of the recent studies characterizing AF blood flow with relatively large cohorts agree that there is a significant decrease of LA flow velocity in both persistent and paroxysmal AF patients

Study	Cohorts (n)	LA Flow parameters	Main Findings
Fluckiger et al. (2013) [53]	PAF (6) Persistent AF (4) Controls (19)	Mean velocity	Mean velocity ↓ in persistent AF cohort
Markl et al. (2016) [54]	AF-sinus (42) AF-afib (39) Young controls (10) Controls (20)	Peak velocity, time-to-peak velocity, stasis	1. Peak velocity ↓ in AF-afib 2. Stasis ↑ in AF-sinus and AF-afib
Lee et al. (2016) [55]	AF (40) Young controls (24) Controls (20)	Velocity (mean, median, and peak)	1. Velocity ↓ (mean and median showed most significant difference) 2. CHA_2DS_2-VASc score inversely correlated with mean, median, and peak velocity
Markl et al. (2016) [56]	AF-sinus (30) AF-afib (30) Controls (15)	Velocity (mean and peak), Stasis (in LA and LAA)	1. Individual variability of flow patterns in AF patients, despite the same CHA_2DS_2-VASc score 2. CHA_2DS_2-VASc correlated positively with stasis, but negatively with velocity
Garcia et al. (2020) [57]	PAF (45) Controls (15)	LA velocity (mean, median, and peak), pulmonary vein peak velocity, stasis, vortex size	1. Mean and median LA velocity ↓, pulmonary vein peak velocity ↓ 2. Stasis ↑ 3. Vortex size ↑ and correlated with CHA_2DS_2-VASc
Kim et al. (2020) [58]	PAF (28) Controls (10)	Peak velocity, delayed ejection, residual volume, regurgitation	1. Residual volume ↓ 2. Delayed ejection ↑
Demirkiran et al. (2021) [59]	PAF (10) Controls (5)	Velocity (mean and peak), stasis (in LA and LAA), KE (mean and peak)	1. Mean/peak velocities ↓ 2. LA and LAA stasis ↑ 3. Mean and peak KE ↓
Spartera et al. (2021) [60]	AF- afib (22) AF-sinus (64)	Velocity (mean and peak), stasis, vorticity, vortex volume	Peak velocity and vorticity are reproducible, stable, and exhibit similar interval-scan variability between cohorts

LA: left atrium; LAA: left atrial appendage; PAF: paroxysmal atrial fibrillation; AF: atrial fibrillation; AF-sinus: previous history of AF, but in sinus rhythm at time of imaging; AF-afib: in AF at time of imaging; KE: kinetic energy; CHA_2DS_2-VASc: stroke risk stratification system that accounts for patient history of congestive heart failure, hypertension, age > 75 years, diabetes mellitus, stroke, vascular disease, age between 64 and 75 years, and sex.

Table 2.
Summary of 4D flow studies in AF.

[54–57, 59]. Most notably, the increase of CHA_2DS_2-VASc score has been associated with reduced mean LA velocity [55, 56], which suggests 4D flow measurement may be able to improve risk assessment. Kinetic energy, which is proportional to the mean square of velocity, was also found to be markedly lower in AF patients than in controls [59]. Left atrial flow stasis is defined by Markl et al. [54] as the relative number of time frames, for each voxel, with flow velocity less than 0.1 m/s. Flow stasis has been confirmed by several studies to be elevated in AF patients [6, 8–10]. An example of a MIP for flow stasis is displayed in **Figure 5**. Also, flow patterns through the pulmonary vein into the LA have been studied [57].

In AF patients, fragmentation of LA inflow and vortex formation in the LA was characterized, see **Figure 6**. This study demonstrated that vortex size increased in paroxysmal AF and was associated with a greater risk score. Similar findings of decreased velocity and increased stasis have also been found in the LAA specifically [56, 59]. However, the limited spatial resolution of 4D flow MRI may not satisfy the minimum number of voxels needed to segment the LAA accurately and reliably in a certain number of cases [6]. In a recent study, reliability and reproducibility of 4D flow parameters in AF patients were reported [60]. Left atrial peak velocity

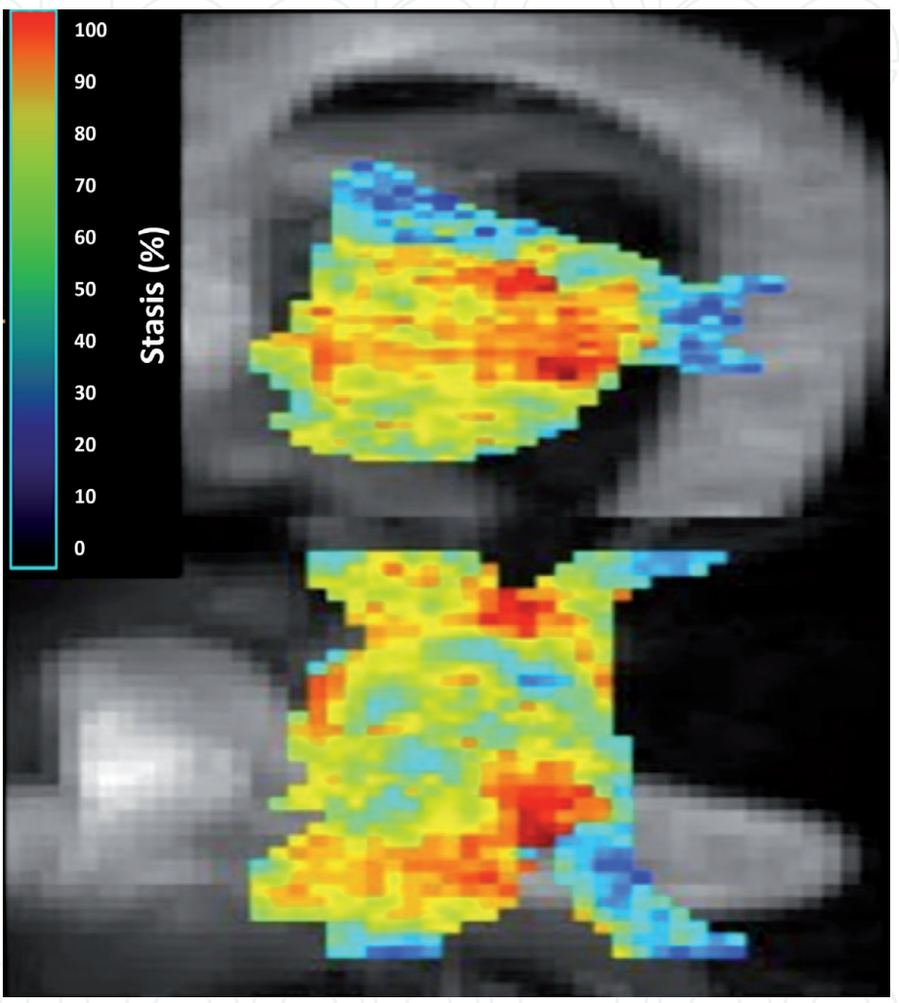

Figure 5.
Left atrial stasis maps. *Maximum intensity projections of stasis using a sagittal-view (top) and a top-view (bottom).*

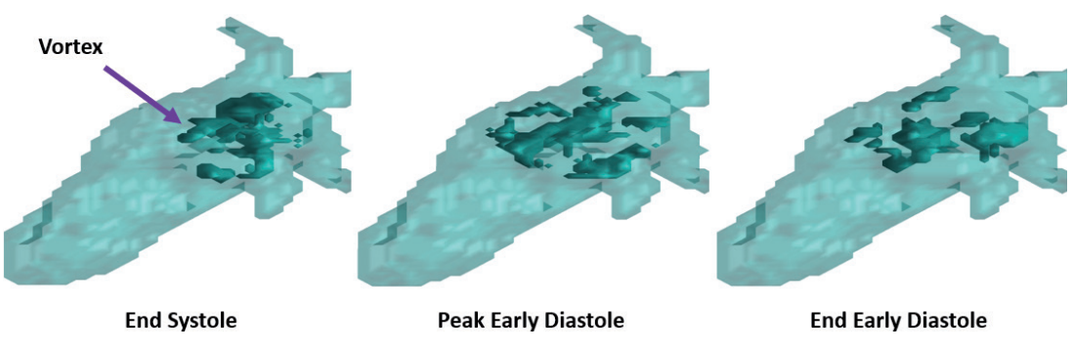

Figure 6.
Atrial vortex dynamics in atrial fibrillation.

and vorticity were found to be more reproducible and independent of physiological factors than mean velocity, vortex volume and stasis.

3.4 Bicuspid aortic valve disease and Aortopathy

Bicuspid aortic valve (BAV) disease is the most common congenital valve disease, affecting 0.5–1.4% of the general population [61–63]. While an aortic valve normally contains three functional leaflets (i.e. tricuspid), a BAV contains only two. There are different sub-types of BAV: valves that developed with only two leaflets (Type 0) and valves that developed with three leaflets containing a fusion between any adjacent pair (Type 1) [64]. Type 1 phenotypes are further subdivided depending on what leaflet pair is fused. Despite being a valvular malformation, BAV disease is closely associated with aortic dilation (BAV aortopathy) that increases patients' risk of aortic aneurysms and dissections [65]. Traditionally, aortic diameters and growth rates have been used to stratify BAV patients at risk for aortic dissection, but these measures alone have been shown to possess limited prognostic value [66]. As well, uncertainties still exist regarding the exact pathophysiology of BAV aortopathy and the most effective timing of surgical intervention [67]. Thus, it is important to study new biomarkers that may enhance our understanding of BAV disease progression. Four-dimensional flow MRI has allowed the study of several new and promising biomarkers, such as abnormal flow patterns, WSS, and energy loss.

Eccentric flow jets and helicity are two characteristics of abnormal flow patterns that have shown strong connections with aortic dilation in BAV patients. A tricuspid aortic valve typically produces a centered systolic jet and bulk flow that is parallel to the ascending aorta, while BAVs tend to produce off-centered systolic jets (eccentric flow jets) that lead to circumferential flow and vortices (helicity). Each BAV phenotype has been shown to produce its own general pattern of jet eccentricity and helicity, and the direction and orientation of these abnormal flow patterns has been associated with patterns of aortic dilation [68–71]. For example, patients with right–left coronary leaflet fusion (Type 1 RL) are more likely to produce a flow jet aimed to the right-anterior wall that associates with dilation focused at the mid-ascending aorta, while right-non coronary leaflet fusion patients (Type 1 RN) tend to produce right-posterior flow jets that associate with diffuse dilation extending to the aortic root and/or arch as well, **Figure 7** [69, 70, 72]. Furthermore, Bissel et al. showed that BAV patients with normal flow jets and non-helical flow patterns tended to have similar aortic diameters to healthy volunteers [73]. While more longitudinal studies are needed to confirm causation, these studies seem to collectively suggest that abnormal flow patterns are connected to aortic dilation in BAV patients.

Wall shear stress, a measure of force exerted on the vessel wall by flowing blood, has consistently shown to be elevated in the ascending aorta of BAV patients [69, 74, 75]. The abnormal flow patterns created by a BAV are likely responsible for these increased WSS forces, and WSS itself has also been associated with regions of aortic dilation (**Figure 7**) [68, 69, 71, 73]. Seminal studies conducted by Bollache et al. and Guzzardi et al. demonstrated a possible physiologic mechanism behind WSS-associated aortic dilation, showing that elevated WSS levels may trigger maladaptive metalloproteinase activity which leads to medial elastin fiber degeneration and overall weaker connective tissue in the aortic wall [76]. Thus, it is thought that elevated WSS, driven by abnormal flow patterns, may be a direct mediator of aortopathy in BAV patients. This ability of 4D flow MRI to visualize flow patterns and quantify WSS may provide future clinical utility in the risk-stratification of BAV patients and identifying appropriate timing for aortic surgery.

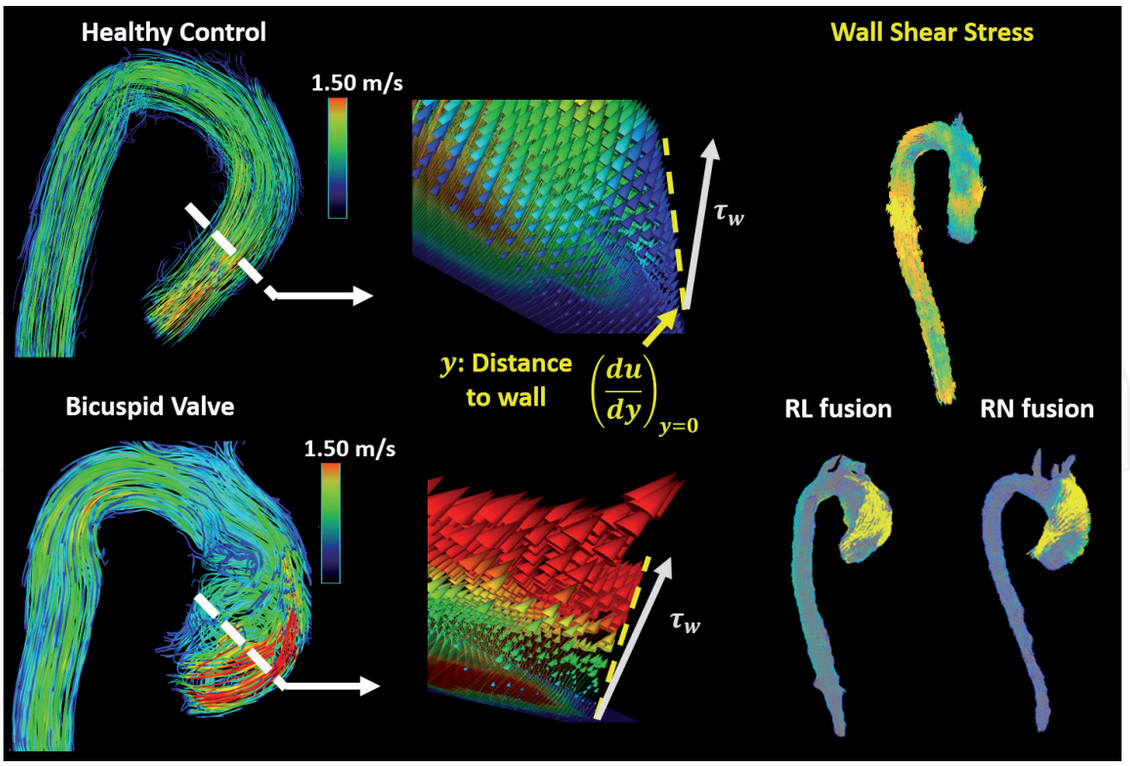

Figure 7.
Flow patterns and wall shear stress in a control and bicuspid valve phenotype. *The white dashed lines represent the location where the sample velocity profile was obtained. These flow profiles can estimate the shear stress rate, blood flow spatial deformation. Since no flow occurs through the vessel wall, the speed of the blood flow at the vessel boundary is zero. The near wall region is the boundary layer where the wall shear stress (WSS) forces occur. The WSS expresses the force per unit area exerted in the fluid direction on the local vessel tangent (τ_w). Yellow dashed lines illustrate the flow profile slope near the wall. On the top, a healthy control illustrates normal flow in the proximal ascending aorta. On the bottom, samples of right–left (RL) fusion and right-non coronary (RN) fusion illustrate abnormal flow.*

3.5 Aortic stenosis

Aortic stenosis (AS) refers to the narrowing of the aortic valve opening, which restricts blood flow from the LV to the aorta. It is the most prevalent valvular disease in developed countries, affecting 2.4% of those >75 years of age [77]. It is commonly a result of BAV disease, chronic calcification, or rheumatic fever (in developing countries). Aortic stenosis often leads to complications such as LV dysfunction, heart failure, and aortic dilation, aneurysm and dissection [78]. Surgical repair or valve replacement are the only known definitive treatments and accurate diagnosis and staging are critical for surgical decision-making [79]. The most widely used parameters in assessing valve function include transvalvular pressure gradient, peak velocity, and valve area. However, up to 40% of AS patients present with discordant findings (ex: abnormally small valve area, but normal pressure gradient) that require additional imaging, and the heterogenous nature of onset of secondary complications (ex: different dilation patterns, different rates of progression, etc.) is not well understood [80]. Four-dimensional flow MRI research continues to enhance our understanding these issues through the novel measurement of 3D peak velocity, 3D pressure gradients, and fluid energy losses.

Peak velocity and pressure gradients across the aortic valve are key components in AS severity grading [79]. However, as previously mentioned, echocardiography and 2D PC-MRI measurements often underestimate peak velocity, due to inaccurate

2D analysis plane placement, and overestimate pressure gradients, due to exclusion of downstream pressure recovery in calculations. The 3D visualization of these parameters using 4D flow MRI allows for more accurate identification of true peak velocity and a comprehensive calculation of pressure gradients that accounts for pressure recovery in the thoracic aorta. Due to this, 4D flow MRI may be a more accurate imaging modality for AS severity grading and surgical decision-making. Although, it should be noted that 3D pressure gradient calculations assume laminar flow, which may lead to inaccuracies when measuring severely stenotic flow where turbulence exists [33].

Fluid energy loss is an advanced hemodynamic parameter that provides information regarding LV workload. There are two types of mutually exclusive fluid energy loss measurements: viscous energy loss (EL; energy lost due to friction between adjacent fluid layers with different velocities) and TKE (energy lost to turbulence) [81]. Both measurements reflect LV output lost to abnormal flow patterns and, ultimately, a greater cardiac afterload. Larger fluid energy losses place greater workloads on the LV, which can lead to LV dysfunction and heart failure. Several studies have shown the presence of significantly elevated fluid energy losses in AS patients and explored the role of TKE in improved characterization of AS severity [82, 83]. Specifically, Binter et al. found TKE to be greater in AS patients compared to controls and demonstrated TKE to be influenced by aortic and valvular morphology [83]. Taken together, this body of research suggests that fluid energy loss may provide novel AS severity measurements that are complimentary to traditional evaluation techniques. Lastly, it should be noted that jet eccentricity, helicity, and WSS measurements may serve the same purpose in the study of AS as they do in the study of BAV disease. These parameters have shown close associations with aortic dilation, a common complication in AS patients [68, 69, 73, 84, 85]. Most studies exploring these associations use BAV patient cohorts, since AS is a common finding in BAV disease.

3.6 Aortic Coarctation

Aortic coarctation (CoA) refers to a congenital narrowing of the thoracic aortic lumen, most often in the arch or descending portion, and accounts for approximately 6–8% of all congenital heart defects [86]. It often accompanies other congenital malformations, such as BAV (60%), aortic arch hypoplasia (18%), ventricular septal defect (13%), and sub AS (6%) [87]. Similar to AS, CoA causes an upstream increase in pressure, which may lead to LV dysfunction, aortic aneurysm and dissection, upper body hypertension, and stroke. Current diagnostics include computed tomographic angiography to image aortic structure and echocardiography to measure peak velocities and pressure gradients across the stenotic region. Due to the limitations of echocardiography, 4D flow MRI may provide added utility in characterizing CoA via 3D measurement of peak velocity profiles and pressure gradients.

The application of 4D flow MRI in generating 3D peak velocity profiles and pressure gradients serves the same benefits as previously mentioned in other cardiovascular disease. That is, it allows the visualization of temporally and spatially resolved flow patterns so that analysis planes may be placed in the most applicable locations and pressure recovery can be accounted for when measuring pressure drop across the CoA (**Figure 8**). Several studies to-date have found benefit in the use of 4D flow MRI for characterizing CoA flow patterns and evaluating post-repair hemodynamics in CoA patients [88–90].

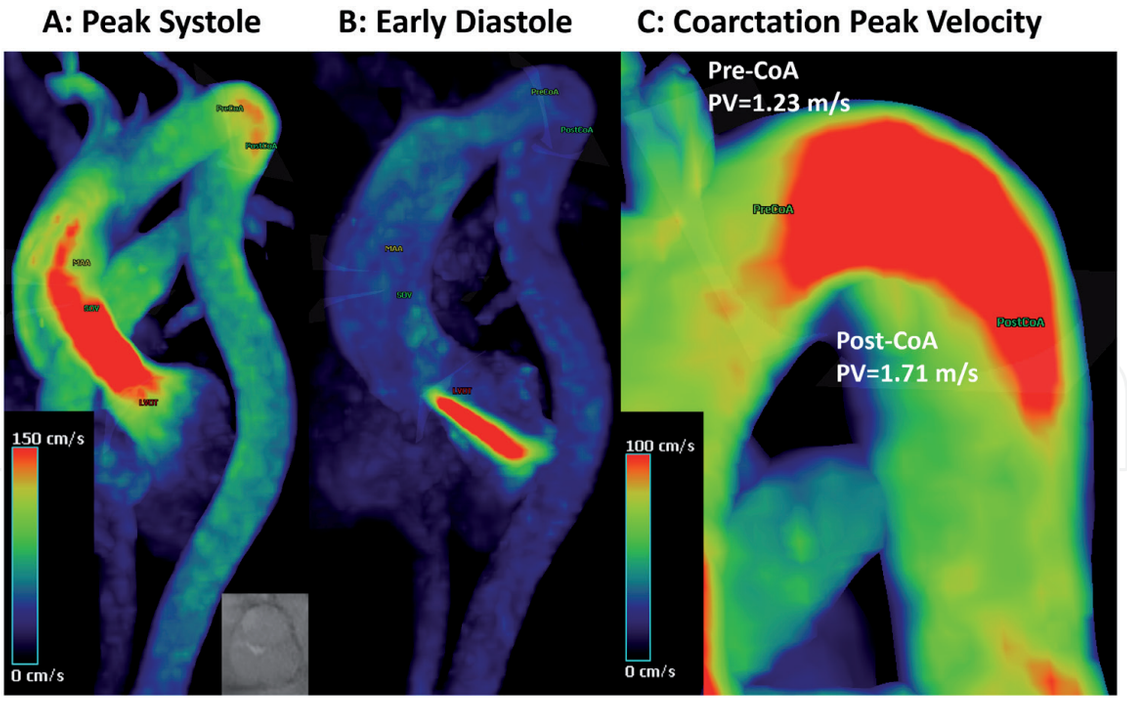

Figure 8.
Evaluation of a coarctation of the aorta. *Flow is visualized at peak systole (A) and early diastole (B). (C) Peak flow velocity (PV) across coarctation. This patient (male, 53 years old) has a type 1 LR BAV with severe aortic insufficiency (regurgitant fraction 56%), mild stenosis, coarctation measuring 21 mm, and moderate dilatation of the proximal ascending aorta (46 mm). LR: Left – Right coronary leaflet fusion; BAV: Bicuspid aortic valve.*

4. Conclusion

In conclusion, 4D flow MRI is a powerful technique which can be used for calculating important clinical parameters. This chapter intended to introduce and summarize the usefulness of 4D flow for assessing cardiovascular diseases. Thanks to recent technical advances, 4D flow MRI has increased its use in cardiac MRI sites worldwide and it is in a ready-to-go state-of-art stage for clinical practicality.

Acknowledgements

Authors were supported by The University of Calgary, URGC SEM #1054341 and JG start-up funding. Research unrestricted funding was also provided by The Libin Cardiovascular Institute and Siemens Healthineers. HK, SIA, and SA received scholarship support from the Biomedical Engineering graduate program. We acknowledge the support of the Natural Science and Engineering Research Council of Canada/Conseil de recherche en science naturelles et en génie du Canada, RGPIN-2020-04549 and DGECR-2020-00204.

Conflict of interest

Authors have no conflict of interest to declare in the context of this chapter.

DOI: http://dx.doi.org/10.5772/intechopen.99362

IntechOpen

Author details

Patrick Geeraert, Hansuk Kim, Safia Ihsan Ali, Ashifa Hudani, Shirin Aliabadi, Monisha Ghosh Srabanti, Hourieh Jamalidinan and Julio Garcia*
University of Calgary, Calgary, Canada

*Address all correspondence to: julio.garciaflores@ucalgary.ca

IntechOpen

References

[1] Otto CM, Nishimura RA, Bonow RO, Carabello BA, Erwin JP, Gentile F, et al. 2020 ACC/AHA Guideline for the Management of Patients With Valvular Heart Disease: Executive Summary. J Am Coll Cardiol. 2021;77(4):450-500.

[2] Fyrenius A, Wigstrom L, Bolger AF, Ebbers T, Ohman KP, Karlsson M, et al. Pitfalls in Doppler evaluation of diastolic function: Insights from 3-dimensional magnetic resonance imaging. J Am Soc Echocardiogr. 1999;12(10):817-826.

[3] Bach DS. Echo/Doppler evaluation of hemodynamics after aortic valve replacement: principles of interrogation and evaluation of high gradients. JACC Cardiovasc Imaging. 2010;3(3):296-304.

[4] Garcia D, Pibarot P, Dumesnil JG, Sakr F, Durand L-G. Assessment of Aortic Valve Stenosis Severity A New Index Based on the Energy Loss Concept. Circulation. 2000;101: 765-771.

[5] Rizk J. 4D flow MRI applications in congenital heart disease. Eur Radiol. 2021 Feb;31(2):1160-1174.

[6] Dyverfeldt P, Bissell M, Barker AJ, Bolger AF, Carlhäll C-J, Ebbers T, et al. 4D flow cardiovascular magnetic resonance consensus statement. J Cardiovasc Magn Reson. 2015;17(1):72.

[7] Stankovic Z, Allen BD, Garcia J, Jarvis KB, Markl M. 4D Flow Imaging with MRI. Cardiovasc Diagn Ther. 2014;4(2):173-192.

[8] Zhong L, Schrauben EM, Garcia J, Uribe S, Grieve SM, Elbaz MSM, et al. Intracardiac 4D Flow MRI in Congenital Heart Disease: Recommendations on Behalf of the ISMRM Flow & Motion Study Group. J Magn Reson Imaging. 2019;50(3):677-681.

[9] Pelc NJ, Herfkens RJ, Shimakawa A, Enzmann DR. Phase contrast cine magnetic resonance imaging. Magn Reson Q. 1991;7(4):229-254.

[10] Wu W, Budovec J, Foley WD. Prospective and retrospective ECG gating for thoracic CT angiography: a comparative study. AJR Am J Roentgenol. 2009;193(4):955-963.

[11] Moghari MH, Roujol S, Chan RH, Hong SN, Bello N, Henningsson M, et al. Free-breathing 3D cardiac MRI using iterative image-based respiratory motion correction. Magn Reson Med. 2013;70(4):1005-1015.

[12] Baltes C, Kozerke S, Hansen MS, Pruessmann KP, Tsao J, Boesiger P. Accelerating cine phase-contrast flow measurements using k-t BLAST and k-t SENSE. Magn Reson Med. 2005;54(6):1430-1438.

[13] Lustig M, Donoho D, Pauly JM. Sparse MRI: The application of compressed sensing for rapid MR imaging. Magn Reson Med. 2007;58(6):1182-1195.

[14] Stadlbauer A, van der Riet W, Crelier G, Salomonowitz E. Accelerated time-resolved three-dimensional MR velocity mapping of blood flow patterns in the aorta using SENSE and k-t BLAST. Eur J Radiol. 2010;75(1):e15-e21.

[15] Keller EJ, Collins JD, Rigsby C, Carr JC, Markl M, Schnell S. Superior Abdominal 4D Flow MRI Data Consistency with Adjusted Preprocessing Workflow and Noncontrast Acquisitions. Acad Radiol. 2017;24(3):350-358.

[16] Yilmaz P, Wallecan K, Kristanto W, Aben JP, Moelker A. Evaluation of a Semi-automatic Right Ventricle Segmentation Method on Short-Axis MR Images. J Digit Imaging. 2018 Oct;31(5):670-679.

[17] Avendi MR, Kheradvar A, Jafarkhani H. A combined deep-learning and deformable-model approach to fully automatic segmentation of the left ventricle in cardiac MRI. Med Image Anal. 2016;30:108-119.

[18] Cong J, Zheng Y, Xue W, Cao B, Li S. MA-Shape: Modality Adaptation Shape Regression for Left Ventricle Segmentation on Mixed MR and CT Images. IEEE Access. 2019;7: 16584-16593.

[19] Huang S, Liu J, Lee LC, Venkatesh SK, Teo LLS, Au C, et al. An image-based comprehensive approach for automatic segmentation of left ventricle from cardiac short axis cine MR images. J Digit Imaging. 2011;24(4):598-608.

[20] Litjens G, Ciompi F, Wolterink JM, de Vos BD, Leiner T, Teuwen J, et al. State-of-the-Art Deep Learning in Cardiovascular Image Analysis. JACC Cardiovasc Imaging. 2019;12(8): 1549-1565.

[21] Ronneberger O, Fischer P, Brox T. U-Net: Convolutional Networks for Biomedical Image Segmentation. In 2015. p. 234-241.

[22] Berhane H, Scott M, Elbaz M, Jarvis K, McCarthy P, Carr J, et al. Fully automated 3D aortic segmentation of 4D flow MRI for hemodynamic analysis using deep learning. Magn Reson Med. 2020;84(4):2204-2218.

[23] Bratt A, Kim J, Pollie M, Beecy AN, Tehrani NH, Codella N, et al. Machine learning derived segmentation of phase velocity encoded cardiovascular magnetic resonance for fully automated aortic flow quantification. J Cardiovasc Magn Reson. 2019;21(1):1.

[24] Wu B, Fang Y, Lai X. Left ventricle automatic segmentation in cardiac MRI using a combined CNN and U-net approach. Comput Med Imaging Graph. 2020;82:101719.

[25] Medicine I of. Cardiovascular disability: Updating the social security listings. Cardiovascular Disability: Updating the Social Security Listings. National Academies Press; 2010. 1-278 p.

[26] Therrien J, Webb G. Clinical update on adults with congenital heart disease. Lancet. 2003;362(9392):1305-1313.

[27] Warmerdam E, Krings GJ, Leiner T, Grotenhuis HB. Three-dimensional and four-dimensional flow assessment in congenital heart disease. Heart. 2020;106(6):421-426.

[28] Ota H, Higuchi S, Sun W, Ueda T, Takase K, Tamura H. Four-Dimensional Flow Magnetic Resonance Imaging for Cardiovascular Imaging: from Basic Concept to Clinical Application. Cardiovasc Imaging Asia. 2018;2(2): 85-96.

[29] Jeong D, Anagnostopoulos P V., Roldan-Alzate A, Srinivasan S, Schiebler ML, Wieben O, et al. Ventricular kinetic energy may provide a novel noninvasive way to assess ventricular performance in patients with repaired tetralogy of Fallot. J Thorac Cardiovasc Surg. 2015;149(5):1339-1347.

[30] Jamalidinan F, Hassanabad AF, François CJ, Garcia J. Four-dimensional-flow Magnetic Resonance Imaging of the Aortic Valve and Thoracic Aorta. Radiol Clin North Am. 2020;58(4): 753-763.

[31] Leidenberger T, Gordon Y, Farag M, Delles M, Fava Sanches A, Fink MA, et al. Imaging-Based 4D Aortic Pressure Mapping in Marfan Syndrome Patients: A Matched Case-Control Study. Ann Thorac Surg. 2020;109(5):1434-1440.

[32] Chelu RG, van den Bosch AE, van Kranenburg M, Hsiao A, van den Hoven AT, Ouhlous M, et al. Qualitative

grading of aortic regurgitation: a pilot study comparing CMR 4D flow and echocardiography. Int J Cardiovasc Imaging. 2016 Feb;32(2):301-307.

[33] Bock J, Frydrychowicz A, Lorenz R, Hirtler D, Barker AJ, Johnson KM, et al. In vivo noninvasive 4D pressure difference mapping in the human aorta: phantom comparison and application in healthy volunteers and patients. Magn Reson Med. 2011;66(4): 1079-1088.

[34] Tyszka JM, Laidlaw DH, Asa JW, Silverman JM. Three-dimensional, time-resolved (4D) relative pressure mapping using magnetic resonance imaging. J Magn Reson Imaging. 2000;12(2):321-329.

[35] Ebbers T, Wigström L, Bolger AF, Wranne B, Karlsson M. Noninvasive measurement of time-varying three-dimensional relative pressure fields within the human heart. J Biomech Eng. 2002;124(3):288-293.

[36] Hassanabad AF, Burns F, Bristow MS, Lydell C, Howarth AG, Heydari B, et al. Pressure drop mapping using 4D flow MRI in patients with bicuspid aortic valve disease: A novel marker of valvular obstruction. Magn Reson Imaging. 2020;65:175-182.

[37] Nkomo VT, Gardin JM, Skelton TN, Gottdiener JS, Scott CG, Enriquez-Sarano M. Burden of valvular heart diseases: a population-based study. Lancet. 2006;368(9540): 1005-1011.

[38] Nishimura RA, Vahanian A, Eleid MF, Mack MJ. Mitral valve disease--current management and future challenges. Lancet. 2016;387(10025):1324-1334.

[39] Ling LH, Enriquez-Sarano M, Seward JB, Tajik AJ, Schaff H V., Bailey KR, et al. Clinical outcome of mitral regurgitation due to flail leaflet. N Engl J Med. 1996;335(19):1417-1423.

[40] Kagiyama N, Shrestha S. Echocardiographic assessment of mitral regurgitation. J Med Ultrason (2001). 2020;47(1):59-70.

[41] Enriquez-Sarano M, Akins CW, Vahanian A. Mitral regurgitation. Lancet. 2009;373(9672):1382-1394.

[42] Heitner J, Bhumireddy GP, Crowley AL, Weinsaft J, Haq SA, Klem I, et al. Clinical application of cine-MRI in the visual assessment of mitral regurgitation compared to echocardiography and cardiac catheterization. PLoS One. 2012;7(7):e40491.

[43] Chew PG, Bounford K, Plein S, Schlosshan D, Greenwood JP. Multimodality imaging for the quantitative assessment of mitral regurgitation. Quant Imaging Med Surg. 2018;8(3):342-359.

[44] Fidock B, Barker N, Balasubramanian N, Archer G, Fent G, Al-Mohammad A, et al. A Systematic Review of 4D-Flow MRI Derived Mitral Regurgitation Quantification Methods. Front Cardiovasc Med. 2019;6:103.

[45] Calkoen EE, Elbaz MSM, Westenberg JJM, Kroft LJM, Hazekamp MG, Roest AAW, et al. Altered left ventricular vortex ring formation by 4-dimensional flow magnetic resonance imaging after repair of atrioventricular septal defects. J Thorac Cardiovasc Surg. 2015;150(5): 1233-40.e1.

[46] Kräuter C, Reiter U, Reiter C, Nizhnikava V, Masana M, Schmidt A, et al. Automated mitral valve vortex ring extraction from 4D-flow MRI. Magn Reson Med. 2020;84(6): 3396-3408.

[47] Calkoen E, de Koning PJ, van der Geest RJ, de Roos A, Westenberg JJ, Roest A. Vortex flow in the left atrium in healthy controls and patients with mitral valve regurgitation after atrioventricular septal defect correction: evaluation with 4D Flow MRI and particle tracing. J Cardiovasc Magn Reson. 2015 Dec 3;17(S1):Q123.

[48] El Sabbagh A, Reddy YN V, Nishimura RA. Mitral Valve Regurgitation in the Contemporary Era: Insights Into Diagnosis, Management, and Future Directions. JACC Cardiovasc Imaging. 2018;11(4):628-643.

[49] Le Goffic C, Toledano M, Ennezat P-V, Binda C, Castel A-L, Delelis F, et al. Quantitative Evaluation of Mitral Regurgitation Secondary to Mitral Valve Prolapse by Magnetic Resonance Imaging and Echocardiography. Am J Cardiol. 2015;116(9):1405-1410.

[50] January CT, Wann LS, Alpert JS, Calkins H, Cigarroa JE, Cleveland JC, et al. 2014 AHA/ACC/HRS guideline for the management of patients with atrial fibrillation: a report of the American College of Cardiology/American Heart Association Task Force on Practice Guidelines and the Heart Rhythm Society. J Am Coll Cardiol. 2014;64(21):e1-76.

[51] Andrade JG, Aguilar M, Atzema C, Bell A, Cairns JA, Cheung CC, et al. The 2020 Canadian Cardiovascular Society/ Canadian Heart Rhythm Society Comprehensive Guidelines for the Management of Atrial Fibrillation. Can J Cardiol. 2020;36(12):1847-1948.

[52] Pamukcu B, Lip GYH, Lane DA. Simplifying stroke risk stratification in atrial fibrillation patients: Implications of the CHA2DS2-VASc risk stratification scores. Age Ageing. 2010;39(5):533-535.

[53] Fluckiger JU, Goldberger JJ, Lee DC, Ng J, Lee R, Goyal A, et al. Left atrial flow velocity distribution and flow coherence using four-dimensional FLOW MRI: a pilot study investigating the impact of age and Pre- and Postintervention atrial fibrillation on atrial hemodynamics. J Magn Reson Imaging. 2013;38(3):580-587.

[54] Markl M, Lee DC, Ng J, Carr M, Carr J, Goldberger JJ. Left Atrial 4-Dimensional Flow Magnetic Resonance Imaging: Stasis and Velocity Mapping in Patients With Atrial Fibrillation. Invest Radiol. 2016;51(3): 147-154.

[55] Lee DC, Markl M, Ng J, Carr M, Benefield B, Carr JC, et al. Three-dimensional left atrial blood flow characteristics in patients with atrial fibrillation assessed by 4D flow CMR. Eur Hear J – Cardiovasc Imaging. 2016;17(11):1259-1268.

[56] Markl M, Lee DC, Furiasse N, Carr M, Foucar C, Ng J, et al. Left Atrial and Left Atrial Appendage 4D Blood Flow Dynamics in Atrial Fibrillation. Circ Cardiovasc Imaging. 2016;9(9): e004984.

[57] Garcia J, Sheitt H, Bristow MS, Lydell C, Howarth AG, Heydari B, et al. Left atrial vortex size and velocity distributions by 4D flow MRI in patients with paroxysmal atrial fibrillation: Associations with age and CHA2 DS2 -VASc risk score. J Magn Reson Imaging. 2020;51(3):871-884.

[58] Kim H, Sheitt H, Jamalidinan F, Wilton S, White J, Garcia J. Left Ventricular Flow Analysis in Atrial Fibrillation. In: 2020 42nd Annual International Conference of the IEEE Engineering in Medicine & Biology Society (EMBC). IEEE; 2020. p. 1182-1185.

[59] Demirkiran A, Amier RP, Hofman MBM, van der Geest RJ, Robbers LFHJ, Hopman LHGA, et al.

Altered left atrial 4D flow characteristics in patients with paroxysmal atrial fibrillation in the absence of apparent remodeling. Sci Rep. 2021;11(1):5965.

[60] Spartera M, Pessoa-Amorim G, Stracquadanio A, Von Ende A, Fletcher A, Manley P, et al. Left atrial 4D flow cardiovascular magnetic resonance: a reproducibility study in sinus rhythm and atrial fibrillation. J Cardiovasc Magn Reson. 2021 Dec 22;23(1):29.

[61] Nistri S, Basso C, Marzari C, Mormino P, Thiene G. Frequency of bicuspid aortic valve in young male conscripts by echocardiogram. Am J Cardiol. 2005;96(5):718-721.

[62] Tutar E, Ekici F, Atalay S, Nacar N. The prevalence of bicuspid aortic valve in newborns by echocardiographic screening. Am Heart J. 2005;150(3): 513-515.

[63] Basso C, Boschello M, Perrone C, Mecenero A, Cera A, Bicego D, et al. An echocardiographic survey of primary school children for bicuspid aortic valve. Am J Cardiol. 2004;93(5):661-663.

[64] Sievers H-H, Schmidtke C. A classification system for the bicuspid aortic valve from 304 surgical specimens. J Thorac Cardiovasc Surg. 2007;133(5):1226-1233.

[65] Masri A, Svensson LG, Griffin BP, Desai MY. Contemporary natural history of bicuspid aortic valve disease: a systematic review. Heart. 2017;103(17):1323-1330.

[66] Linda AP, Thomas TT, Eric MI, others. Aortic diameter≥ 5.5 cm is not a good predictor of type a aortic dissection: observations from the International Registry of Acute Aortic Dissection (IRAD). Circulation. 2007;116(10):1120-1127.

[67] Borger MA, Fedak PWM, Stephens EH, Gleason TG, Girdauskas E, Ikonomidis JS, et al. The American Association for Thoracic Surgery consensus guidelines on bicuspid aortic valve–related aortopathy: Full online-only version. J Thorac Cardiovasc Surg. 2018;156(2):e41–e74.

[68] Rodríguez-Palomares JF, Dux-Santoy L, Guala A, Kale R, Maldonado G, Teixidó-Turà G, et al. Aortic flow patterns and wall shear stress maps by 4D-flow cardiovascular magnetic resonance in the assessment of aortic dilatation in bicuspid aortic valve disease. J Cardiovasc Magn Reson. 2018;20(1):28.

[69] Mahadevia R, Barker AJ, Schnell S, Entezari P, Kansal P, Fedak PWM, et al. Bicuspid aortic cusp fusion morphology alters aortic three-dimensional outflow patterns, wall shear stress, and expression of aortopathy. Circulation. 2014;129(6):673-682.

[70] Garcia J, Barker AJ, Collins JD, Carr JC, Markl M. Volumetric quantification of absolute local normalized helicity in patients with bicuspid aortic valve and aortic dilatation. Magn Reson Med. 2017;78(2):689-701.

[71] Dux-Santoy L, Guala A, Teixidó-Turà G, Ruiz-Muñoz A, Maldonado G, Villalva N, et al. Increased rotational flow in the proximal aortic arch is associated with its dilation in bicuspid aortic valve disease. Eur Hear Journal-Cardiovascular Imaging. 2019;20(12):1407-1417.

[72] Fatehi Hassanabad A, Garcia J, Verma S, White JA, Fedak PWM. Utilizing wall shear stress as a clinical biomarker for bicuspid valve-associated aortopathy. Curr Opin Cardiol. 2019;34(2):124-131.

[73] Bissell MM, Hess AT, Biasiolli L, Glaze SJ, Loudon M, Pitcher A, et al. Aortic dilation in bicuspid aortic valve disease: flow pattern is a major contributor and differs with valve fusion type. Circ Cardiovasc Imaging. 2013;6(4):499-507.

[74] Meierhofer C, Schneider EP, Lyko C, Hutter A, Martinoff S, Markl M, et al. Wall shear stress and flow patterns in the ascending aorta in patients with bicuspid aortic valves differ significantly from tricuspid aortic valves: a prospective study. Eur Heart J Cardiovasc Imaging. 2013;14(8):797-804.

[75] van Ooij P, Markl M, Collins JD, Carr JC, Rigsby C, Bonow RO, et al. Aortic Valve Stenosis Alters Expression of Regional Aortic Wall Shear Stress: New Insights From a 4-Dimensional Flow Magnetic Resonance Imaging Study of 571 Subjects. J Am Heart Assoc. 2017;6(9).

[76] Guzzardi DG, Barker AJ, Van Ooij P, Malaisrie SC, Puthumana JJ, Belke DD, et al. Valve-related hemodynamics mediate human bicuspid aortopathy: insights from wall shear stress mapping. J Am Coll Cardiol. 2015;66(8):892-900.

[77] Lindroos M, Kupari M, Heikkilä J, Tilvis R. Prevalence of aortic valve abnormalities in the elderly: An echocardiographic study of a random population sample. J Am Coll Cardiol. 1993;21(5):1220-1225.

[78] Vahanian A, Baumgartner H, Bax J, Butchart E, Dion R, Filippatos G, et al. Guidelines on the management of valvular heart disease: The Task Force on the Management of Valvular Heart Disease of the European Society of Cardiology. Eur Heart J. 2006;28(2): 230-268.

[79] Nishimura RA, Otto CM, Bonow RO, Carabello BA, Erwin JP, Fleisher LA, et al. 2017 AHA/ACC Focused Update of the 2014 AHA/ACC Guideline for the Management of Patients With Valvular Heart Disease: A Report of the American College of Cardiology/American Heart Association Task Force on Clinical Practice Guidelines. J Am Coll Cardiol. 2017;70(2):252-289.

[80] Minners J, Allgeier M, Gohlke-Baerwolf C, Kienzle R-P, Neumann F-J, Jander N. Inconsistent grading of aortic valve stenosis by current guidelines: haemodynamic studies in patients with apparently normal left ventricular function. Heart. 2010;96(18):1463-1468.

[81] Dyverfeldt P, Hope MD, Tseng EE, Saloner D. Magnetic resonance measurement of turbulent kinetic energy for the estimation of irreversible pressure loss in aortic stenosis. JACC Cardiovasc Imaging. 2013;6(1):64-71.

[82] Barker AJ, van Ooij P, Bandi K, Garcia J, Albaghdadi M, McCarthy P, et al. Viscous energy loss in the presence of abnormal aortic flow. Magn Reson Med. 2014 Sep;72(3):620-628.

[83] Binter C, Gotschy A, Sündermann SH, Frank M, Tanner FC, Lüscher TF, et al. Turbulent Kinetic Energy Assessed by Multipoint 4-Dimensional Flow Magnetic Resonance Imaging Provides Additional Information Relative to Echocardiography for the Determination of Aortic Stenosis Severity. Circ Cardiovasc Imaging. 2017;10(6).

[84] Garcia J, Barker AJ, Murphy I, Jarvis K, Schnell S, Collins JD, et al. Four-dimensional flow magnetic resonance imaging-based characterization of aortic morphometry and haemodynamics: impact of age, aortic diameter, and valve morphology. Eur Hear J – Cardiovasc Imaging. 2016;17(8):877-884.

[85] Hope MD, Sigovan M, Wrenn SJ, Saloner D, Dyverfeldt P. MRI hemodynamic markers of progressive bicuspid aortic valve-related aortic disease. J Magn Reson Imaging. 2014;40(1):140-145.

[86] Baumgartner H, Bonhoeffer P, De Groot NMS, de Haan F, Deanfield JE, Galie N, et al. ESC Guidelines for the management of grown-up congenital heart disease (new version 2010). Eur Heart J. 2010;31(23):2915-2957.

[87] Teo LLS, Cannell T, Babu-Narayan S V., Hughes M, Mohiaddin RH. Prevalence of associated cardiovascular abnormalities in 500 patients with aortic coarctation referred for cardiovascular magnetic resonance imaging to a tertiary center. Pediatr Cardiol. 2011;32(8):1120-1127.

[88] Hope MD, Meadows AK, Hope T a, Ordovas KG, Saloner D, Reddy GP, et al. Clinical evaluation of aortic coarctation with 4D flow MR imaging. J Magn Reson Imaging. 2010;31(3):711-718.

[89] Riesenkampff E, Fernandes JF, Meier S, Goubergrits L, Kropf S, Schubert S, et al. Pressure fields by flow-sensitive, 4D, velocity-encoded CMR in patients with aortic coarctation. JACC Cardiovasc Imaging. 2014;7(9):920-926.

[90] Frydrychowicz A, Markl M, Hirtler D, Harloff A, Schlensak C, Geiger J, et al. Aortic hemodynamics in patients with and without repair of aortic coarctation: in vivo analysis by 4D flow-sensitive magnetic resonance imaging. Invest Radiol. 2011;46(5):317-325.